Nonexponential Tunneling due to Mean-Field-Induced Swallowtails

Q. Guan,[1,2] M. K. H. Ome,[3] T. M. Bersano,[3] S. Mossman,[3] P. Engels,[3] and D. Blume[1,2]
[1]Homer L. Dodge Department of Physics and Astronomy, The University of Oklahoma, 440 W. Brooks Street, Norman, Oklahoma 73019, USA
[2]Center for Quantum Research and Technology, The University of Oklahoma, 440 W. Brooks Street, Norman, Oklahoma 73019, USA
[3]Department of Physics and Astronomy, Washington State University, Pullman, Washington 99164-2814, USA

(Received 17 July 2020; accepted 27 October 2020; published 20 November 2020)

Typically, energy levels change without bifurcating in response to a change of a control parameter. Bifurcations can lead to loops or swallowtails in the energy spectrum. The simplest quantum Hamiltonian that supports swallowtails is a nonlinear 2×2 Hamiltonian with nonzero off-diagonal elements and diagonal elements that depend on the population difference of the two states. This work implements such a Hamiltonian experimentally using ultracold atoms in a moving one-dimensional optical lattice. Self-trapping and nonexponential tunneling probabilities, a hallmark signature of band structures that support swallowtails, are observed. The good agreement between theory and experiment validates the optical lattice system as a powerful platform to study, e.g., Josephson junction physics and superfluidity in ring-shaped geometries.

DOI: 10.1103/PhysRevLett.125.213401

In time-dependent processes, two limiting scenarios are of particular interest: the regime where the system Hamiltonian is quenched (i.e., changed essentially instantaneously) and the opposite regime where the system Hamiltonian is changed adiabatically (i.e., so slowly that transitions between different adiabatic eigenstates are strongly suppressed). Generally, the adiabatic regime is reached when the ramp rate α, with which the control parameter γ is changed, is sufficiently small compared to the rate that is set by the energy gap Ω (Ω is taken to be real) at the avoided crossing of neighboring adiabatic eigenstates. This is captured by the celebrated "linear" Landau-Zener formula [1,2], which gives the tunneling probability r between two energy levels, assuming γ changes linearly with time t [$\gamma(t) = \alpha t$, $\alpha > 0$],

$$r = \exp\left[-\pi\Omega^2/(2\hbar\alpha)\right]. \tag{1}$$

According to the Landau-Zener formula, adiabaticity (i.e., the $r \to 0$ limit) can always be approached, at least in principle, by reducing the ramp rate α.

The presence of a nonlinearity C alters the tunneling dynamics qualitatively and quantitatively [3–18]. Adiabaticity breaks down for certain parameter combinations of the nonlinear two-state model, i.e., even an infinitely slow ramp induces nonadiabatic population transfer between states, and the tunneling probability is not given by the "standard exponential" [5]. The breakdown of adiabaticity is intimately linked to the phenomenon of hysteresis and the existence of swallowtails in the adiabatic energy levels of the nonlinear two-state model [8,19]. Mapping to a classical Hamiltonian shows that the swallowtail structure emerges when two new fixed points, one stable and the other unstable, are first supported for $\gamma = \gamma_{c,1}$ [inset of Fig. 1(a)] [5,20]. As the control parameter γ crosses $\gamma_{c,2}$ ($\gamma_{c,2} > \gamma_{c,1}$), a stable and an unstable fixed point

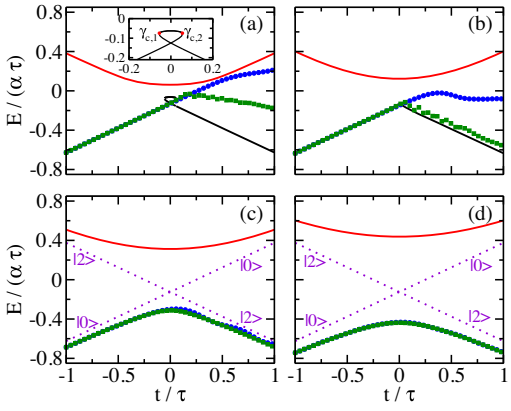

FIG. 1. Scaled energy levels of $\hat{H}_{\rm TS}$ for $C/(\alpha\tau) = 0.268$ as a function of t/τ for (a) $C/\Omega = 2.14$, (b) 1.07, (c) 0.428, and (d) 0.306. Black and red solid lines show the adiabatic energy levels [in (c) and (d), the black lines are covered by the symbols]. Blue circles and green squares show the dynamic energy levels for $\hbar/(\alpha\tau^2) = 7.68 \times 10^{-2}$ and $\hbar/(\alpha\tau^2) = 7.68 \times 10^{-3}$, respectively [in (d), the blue circles are covered by the green squares]. The tunneling probability is appreciable in (a) and (b) and essentially zero in (c) and (d). The inset in (a) shows an enlargement of the swallowtail; $\gamma_{c,1}/(\alpha\tau)$ and $\gamma_{c,2}/(\alpha\tau)$ correspond to the boundaries of the swallowtail. Purple dotted lines in (c) and (d) show the adiabatic energy levels, labeled by their eigenstates, for $\Omega = 0$. The parameters used to make the solid lines and blue circles are the same as those used in Fig. 2.

collide and annihilate. The diverging period of the associated trajectory is responsible for deviations from adiabaticity [5]. While the nonlinear two-state model captures aspects of a wide range of systems such as the motion of small polarons [21,22], Josephson junctions [23–25], helium and other superfluids in annular rings [19,26–29], and Bose-Einstein condensates (BECs) in optical lattices [30–33], nonexponential tunneling originating from swallowtails has not yet been demonstrated experimentally.

Using ultracold ^{87}Rb atoms in a moving one-dimensional optical lattice, the present joint experiment-theory study investigates two-state dynamics in the presence of swallowtails. The main results are as follows: First, a breakdown of adiabaticity is observed. The experimental data are reproduced by mean-field Gross-Pitaevskii (GP) equation simulations and interpreted in terms of self-trapping due to mean-field interactions. Second, nonexponential tunneling probabilities are observed for parameter combinations for which the adiabatic band structure supports swallowtails. Third, intriguing density deformations are revealed.

Consider the time-dependent Schrödinger equation [3] $\imath\hbar\partial_t\vec{b}(t)=\hat{H}_{\mathrm{TS}}\vec{b}(t)$, where the nonlinear 2×2 Hamiltonian $\hat{H}_{\mathrm{TS}}$ with nonlinearity C is given by

$$\hat{H}_{\mathrm{TS}}=\frac{1}{2}\begin{pmatrix}\gamma(t)-C\Delta b(t) & \Omega\\ \Omega & -\gamma(t)+C\Delta b(t)\end{pmatrix} \quad (2)$$

and the state vector $\vec{b}(t)$ by $\vec{b}(t)=[b_0(t),b_2(t)]^T$. The subscripts 0 and 2 are used since our experimental realization connects two sites of a momentum lattice, one with momentum zero and one with momentum $2\hbar k_L$ [5], where k_L denotes the lattice wave vector. In Eq. (2), $\Delta b(t)$ denotes the population imbalance, $\Delta b(t)=|b_0(t)|^2-|b_2(t)|^2$ with normalization $|b_0(t)|^2+|b_2(t)|^2=1$. For $-\tau\le t\le\tau$, the control parameter $\gamma(t)$ changes linearly from $\gamma=-\alpha\tau$ to $\alpha\tau$.

We first consider the case of vanishing nonlinearity ($C=0$). Starting in state $\vec{b}(t)=(1,0)^T\equiv|0\rangle$ at $t=-\tau$, the probabilities to be in states $|0\rangle$ and $|2\rangle\equiv(0,1)^T$ at time τ are given by r and $1-r$, respectively, in the $\tau\to\infty$ limit. In practice, τ is finite and the finite time window defines the "dynamic" energy scale U_d, $U_d=\hbar/\tau$ [34]. In addition, $\hat{H}_{\mathrm{TS}}$ is characterized by the "static" energy scale U_s, $U_s=\alpha\tau$, and the coupling strength Ω. Equation (1) provides—"on average"—a reliable description of the state populations at the end of the ramp if $\Omega/(\alpha\tau)\ll 1$; we use the term on average since the finite time window introduces oscillations around the smooth exponential given in Eq. (1) [34].

We now turn to the nonlinear two-state model. Solid lines in Fig. 1 show the adiabatic energy levels of $\hat{H}_{\mathrm{TS}}$ for $C/(\alpha\tau)=0.268$ as a function of t/τ for four different C/Ω. The band structure displays a swallowtail centered at $t=0$ for $C/\Omega>1$ but not for $C/\Omega<1$. Blue circles and green squares show the dynamic energy levels of $\hat{H}_{\mathrm{TS}}$ [3] for two different ramp rates, parametrized by the scale ratio $\hbar/(\alpha\tau^2)$ [34]. For a given parameter combination, the dynamic energy level is obtained by calculating the energy expectation value at each time, using the lower adiabatic eigenstate of $\hat{H}_{\mathrm{TS}}$ for $\gamma=-\alpha\tau$ as the initial state [3]. In Figs. 1(c) and 1(d), the dynamic energy levels depend rather weakly on the ramp rate and agree well with the lower adiabatic energy levels. In this case, the probability to tunnel to the upper adiabatic energy level during the ramp is very close to zero. In Figs. 1(a) and 1(b), in contrast, the dynamic energy levels depend on $\hbar/(\alpha\tau^2)$ and deviate, even for the smaller $\hbar/(\alpha\tau^2)$ considered (this corresponds, for fixed $\alpha\tau$, to a slower ramp [34]), from the lower adiabatic energy level. Deviations persist even for infinitely slow ramp rates [3], i.e., the probability to tunnel to the upper adiabatic energy level during the ramp is nonzero.

Following earlier experimental work [10,12], we realize the nonlinear Landau-Zener model by preparing a single-component BEC consisting of N ^{87}Rb atoms of mass m in the $|F,m_F\rangle=|1,-1\rangle$ hyperfine state in an optical dipole trap and by then adiabatically loading the BEC into a one-dimensional optical lattice $V_{\mathrm{lat}}(z)$ [36–39]. While the largest C/Ω reported in the literature is around 0.7 [12], we access the $C/\Omega>1$ regime, where swallowtails exist. Our optical lattice is created by two 1064 nm beams [with wave vectors $\vec{k}_1$ and $\vec{k}_2$, $|\vec{k}_1|=|\vec{k}_2|$, and angular frequencies $\omega_1(t)$ and $\omega_2(t)$] that cross at an angle of $\approx\pi/2$, $V_{\mathrm{lat}}(z,t)=2\Omega\cos^2[k_Lz-\phi(t)/2]$; Ω denotes the effective coupling strength, $k_L\approx|\vec{k}_1|/\sqrt{2}$, $\phi(t)=[\omega_1(t)-\omega_2(t)]t$ with $\phi(t)=0$ for $t<-\tau$, and $\delta_L(t)=\hbar\partial_t\phi(t)$. At $t=-\tau$, the optical dipole trap is turned off and the BEC, which has a vanishing momentum, sits in the middle of the first Brillouin zone (state $|0\rangle$). In our first set of experiments, $\delta_L(t)$ is—for $t>-\tau$—increased linearly from 0 with ramp rate $\alpha=h\times 9$ kHz/ms. The time sequence is designed such that $\delta_L(0)$ is equal to 4 E_L and $\delta_L(\tau)$ is equal to 8 E_L, i.e., such that the edge of the first Brillouin zone and the middle of the second Brillouin zone are reached when $t=0$ and $t=\tau$, respectively [here, $E_L=\hbar^2k_L^2/(2m)=h\times 1.08$ kHz]. In each repetition of the experiment, the ramp is stopped at various t and the occupations of the components centered at vanishing momentum along the z direction (state $|0\rangle$) and centered at momentum $2\hbar k_L$ (state $|2\rangle$) are measured after 16.5 ms time of flight, counted from the end of the ramp. During the time-of-flight expansion, the two momentum components separate fully in real space. The turn-off of the lattice beams is essentially instantaneous on all relevant timescales so that the populations of the momentum components are unaffected by the "lattice quench"; effectively, the measurement is made in the diabatic basis. Red circles in Fig. 2 show the experimentally determined population imbalance $\Delta b(t)$. It can be seen that the BEC occupies, for $t/\tau\gtrsim 0$, primarily

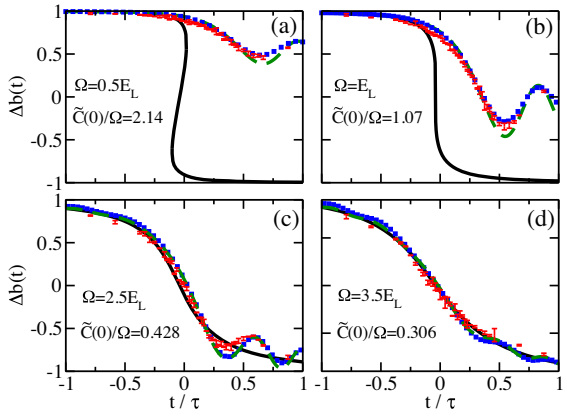

FIG. 2. Experiment-theory comparison of population imbalance $\Delta b(t)$ for a linear ramp with $\alpha = h \times 9\,\mathrm{kHz/ms}$ [$\hbar/(\alpha\tau^2) = 7.68 \times 10^{-2}$] as a function of t/τ for various $\tilde{C}(0)/\Omega$. The experimental results (red error bars show the standard deviation from two independent runs) are for $N = 3.1 \times 10^5$, $\omega_{x,y,z} = 2\pi \times (147, 160, 29.8)$ Hz, and $E_L = h \times 1.08$ kHz. Blue squares and green dashed lines are obtained from $\hat{H}_{\mathrm{GP}}$ and $\hat{H}_{\mathrm{TS},t}$, respectively (analyzing the dynamic states). In both cases, the initial state is prepared in an axially symmetric trap with $\omega_\rho = (\omega_x + \omega_y)/2$. The mean-field energy $\tilde{C}(t)$ is equal to 1.27 E_L and 1.07 E_L for $t = -\tau$ and $t = 0$, respectively. Black solid lines show $\Delta b(t)$ for the lower adiabatic eigenstate of $\hat{H}_{\mathrm{TS},t}$.

state $|2\rangle$ when Ω is "large" and primarily state $|0\rangle$ when Ω is "small."

The lattice system is described by the time-dependent GP equation with Hamiltonian $\hat{H}_{\mathrm{GP}}$ [37],

$$\hat{H}_{\mathrm{GP}} = \hat{\vec{p}}^2/(2m) + V_{\mathrm{lat}}(z,t) + g(N-1)|\Psi(\vec{r},t)|^2. \quad (3)$$

Here, g is equal to $4\pi\hbar^2 a_s/m$ and the mean-field orbital $\Psi(\vec{r},t)$ is normalized according to $\int |\Psi(\vec{r},t)|^2 d\vec{r} = 1$. The s-wave scattering length a_s is equal to 100.4 a_{bohr} [40]. Following the experimental protocol, blue squares in Fig. 2 show our GP mean-field results. The good agreement with the experimental data, including the reproduction of the oscillatory behavior of the population imbalance for $t \gtrsim 0$ and the small deviations of the population imbalance from 1 for large Ω near $t \approx -\tau$, indicate that the mean-field framework captures the dynamics quite accurately.

To bring out the two-state nature of the lattice system, we write [3,4,36] $\Psi(\vec{r},t) = \psi_0(\vec{r},t) + \psi_2(\vec{r},t)\exp(2\imath k_L z)$. Inserting the ansatz into the time-dependent GP equation, the Supplemental Material [34] develops a semianalytical framework that yields a spatially independent two-state Hamiltonian $\hat{H}_{\mathrm{TS},t}$. The Hamiltonian $\hat{H}_{\mathrm{TS},t}$ is identical to $\hat{H}_{\mathrm{TS}}$ provided the mapping $\gamma(t) \to -4E_L + \delta_L(t)$ and $C \to \tilde{C}(t)$ is applied. The time-dependent mean-field energy $\tilde{C}(t)$, $\tilde{C}(t) = g(N-1)\bar{n}(t)$, accounts for the fact that the BEC expands during the ramp, thereby resulting in a decrease of the mean density $\bar{n}(t)$ with increasing $\gamma(t)$. Since we are interested in nonlinear effects, the decrease of the mean-field energy during the ramp places a constraint on α for a given $\tilde{C}(-\tau)/\Omega$. Figure S1 [34] shows the adiabatic and dynamic energy levels of the Hamiltonian $\hat{H}_{\mathrm{TS},t}$ for the experimental parameters used in Fig. 2. Comparison with Fig. 1 shows that the adiabatic and dynamic energy levels supported by $\hat{H}_{\mathrm{TS}}$ and $\hat{H}_{\mathrm{TS},t}$ agree quite well.

Black solid and green dashed lines in Fig. 2 show the decomposition of the states corresponding to, respectively, the lower adiabatic and lower dynamic energy levels supported by $\hat{H}_{\mathrm{TS},t}$. It can be seen that the green dashed lines agree reasonably well with the experimental and GP results; this confirms the applicability of the nonlinear two-state Hamiltonian to the lattice system. Moreover, it can be seen that the decomposition of the states corresponding to the adiabatic and dynamic energy levels agree for the largest Ω value considered [Fig. 2(d)] but differ for the other Ω values. This shows that the system dynamics are, for fixed ramp rate α, adiabatic for the largest Ω considered in Fig. 2 but not for the other Ω values. In Fig. 2(c), the experimental data and populations extracted from the dynamic energy level oscillate around the populations extracted from the adiabatic energy level [41]. In Figs. 2(a) and 2(b), the experimental data and populations extracted from the dynamic energy level oscillate as well for $t \gtrsim 0$; however, the oscillations are not centered around the populations extracted from the adiabatic energy level but instead lie notably above. Our theory analysis shows that the enhanced tunneling probability (enhanced probability to remain in state $|0\rangle$) is due to self-trapping, a phenomenon inherently linked to the presence of swallowtails [30].

While the inhibition of transitions to state $|2\rangle$ due to nonlinear interactions has been previously observed in an optical lattice system similar to ours [17] as well as in coupled double-well type setups [16,42,43] and annular rings [19], we now show evidence for nonexponential tunneling. Earlier work quantified the modifications of the exponential tunneling exponent in the $\tilde{C}(0)/\Omega < 1$ regime using optical lattices but did not observe nonexponential tunneling, which requires $\tilde{C}(0)/\Omega > 1$. Red circles in Fig. 3 show the experimentally measured population of state $|0\rangle$ for $t = \tau$ and $\tilde{C}(-\tau)/\Omega = 2.75$. It can be seen that the experimental data, which are obtained by varying the ramp rate α (and correspondingly τ such that $\alpha\tau$ is equal to 4 E_L), display an overall decrease with increasing $\pi\Omega^2/(2\hbar\alpha)$. The experimental data are quite well reproduced by our GP simulations (blue squares). The decomposition of the state corresponding to the lower dynamic energy level of $\hat{H}_{\mathrm{TS},t}$ (green dashed line) yields notably larger oscillations but displays the same overall trend. In the $\tau \to \infty$ limit, the tunneling probability of the nonlinear two-state model $\hat{H}_{\mathrm{TS}}$ varies nonexponentially with $\pi\Omega^2/(2\hbar\alpha)$ [34]. The gray-shaded region shows the results

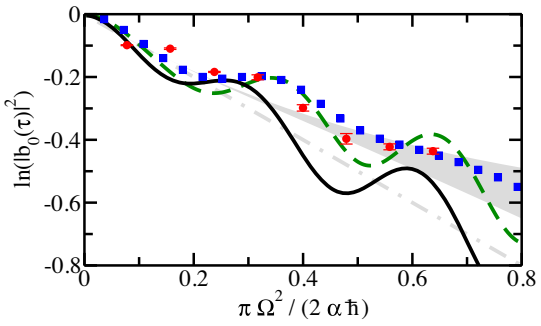

FIG. 3. Experiment-theory comparison of tunneling probability $|b_0(t)|^2$ at $t = \tau$ for linear ramps with varying α for $\tilde{C}(-\tau)/\Omega = 2.75$ as a function of $\pi\Omega^2/(2\hbar\alpha)$. The experimental results (red circles; error bars show the standard deviation from three independent runs) are for $N = 2.3 \times 10^5$, $\omega_{x,y,z} = 2\pi \times (193, 218, 29.8)$ Hz, $E_L = h \times 1.08$ kHz, and $\Omega = 0.52\ E_L$. Blue squares and green dashed lines are obtained for $\hat{H}_{\mathrm{GP}}$ and $\hat{H}_{\mathrm{TS},t}$, respectively [analyzing the dynamic states; the initial state is prepared in an axially symmetric trap with $\omega_\rho = (\omega_x + \omega_y)/2$]. Both datasets follow the nonexponential trend of the gray-shaded region, which shows Eq. (S11) for C/Ω values ranging from $\tilde{C}(-\tau)/\Omega$ to $\tilde{C}(0)/\Omega$ [34]. The black solid line, which oscillates around the linear Landau-Zener formula [gray dash-dotted line; Eq. (1)], shows the tunneling probability for $\hat{H}_{\mathrm{TS}}$ with $C = 0$. The experimental data are better described by the nonexponential gray-shaded family of curves than by the linear Landau-Zener formula.

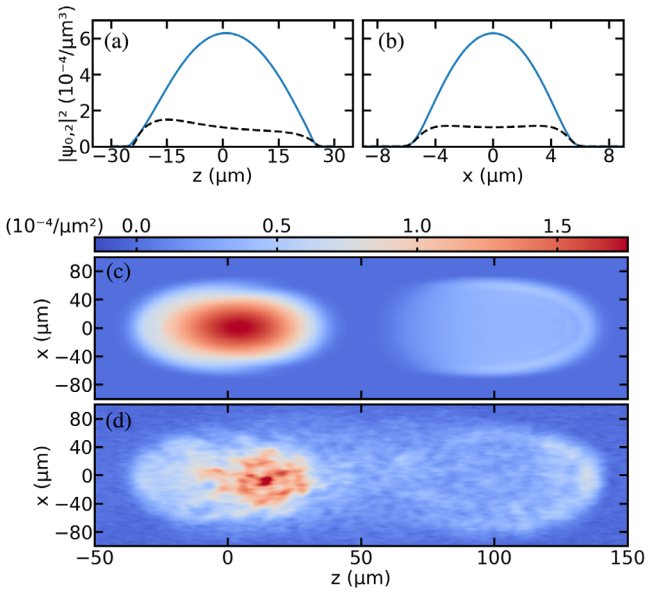

FIG. 4. Theoretical GP and experimental densities for the ramp ending at $t = -\tau + 0.6$ ms [$t/\tau = 0.25$ in Fig. 2(b)]. (a) and (b) Density cuts before time-of-flight expansion for $\rho = 0$ and $y = z = 0$, respectively. Blue solid and black dashed lines are for states $\psi_0(\vec{r}, t)$ and $\psi_2(\vec{r}, t)$, respectively. Panels (c) and (d) show, respectively, the theoretical and experimental integrated densities $n(x, z, t)$, $n(x, z, t) = \int_{-\infty}^{\infty} |\Psi(\vec{r}, t)|^2 dy$, after 16.5 ms time-of-flight expansion.

for C/Ω values between $\tilde{C}(-\tau)/\Omega = 2.75$ (upper bound) and $\tilde{C}(0)/\Omega$ (lower bound; this value varies with the ramp rate), respectively. The experimental and GP data exhibit small oscillations around the gray region, which can be viewed as a "smoothed" version of the green-dashed line. For comparison, the black solid line shows the results for the noninteracting two-state model. Because of the finite time window, the black solid line oscillates around the "linear Landau-Zener" formula [Eq. (1), gray dash-dotted line]. A key observation of our work is that the experimental data are much better described by the nonexponential gray-shaded region than the linear Landau-Zener formula. Figure 3 provides the first experimental verification of nonexponential tunneling dynamics, driven by swallowtails.

Figure 3 also shows that the oscillation amplitude of $\ln[|b_0(t)|^2]$ is smaller for the experimental and GP data than for the finite-τ two-state model data. We attribute this to structural dynamics, which are not accounted for by the two-state models $\hat{H}_{\mathrm{TS}}$ and $\hat{H}_{\mathrm{TS},t}$. Figures 4(a) and 4(b) show GP densities for the ramp stopped at $t/\tau = 0.25$ in Fig. 2(b) (no time-of-flight expansion). The density cuts for the finite momentum component deviate from a simple Thomas-Fermi profile; in particular, the density along z for $\rho = 0$ is deformed, exhibiting a maximum at negative z, and the density along x for $y = z = 0$ exhibits a double peak structure [black dashed lines in Figs. 4(a) and 4(b), respectively]. These density deformations develop during the ramp and are attributed to the interplay between the on-site and off-site mean-field interactions [34]. We emphasize that the employed ramps are faster than the characteristic timescale of a dynamical instability that exists at the edge of the Brillouin zone [44–48]. Whether or not the observed density deformations can be interpreted as a comparatively gentle, nondestructive fingerprint of such a dynamical instability is an open question that deserves further investigation.

Figures 4(c) and 4(d) show GP and experimentally measured integrated densities after 16.5 ms time-of-flight expansion for the same ramp as considered in Figs. 4(a) and 4(b). The overall agreement between theory and experiment is excellent. The zero-momentum component (centered around $z = 0$) has its maximum at positive z while the finite-momentum component (centered around $z \approx 100\ \mu$m) displays an enhanced density that is located on a half-ring on the right edge of the cloud. During the time-of-flight expansion, the finite-momentum component moves relative to the zero-momentum component: To reduce mean-field interactions, the finite-momentum component accumulates density first at the left edge of the cloud and later at the right edge of the cloud. The theory data indicate that the relative motion of the two clouds generates low energy excitations [wavelike density pattern in Fig. 4(c)]; although not clearly resolved,

faint indications of these patterns are visible in the experimental images.

Quantum tunneling is ubiquitous in physics: it plays a central role in high-energy, nuclear, atomic, and condensed matter physics as well as in chemistry, biology, and engineering. Modern physics courses introduce students to quantum tunneling and exponentially decaying tunneling probabilities. The full quantum treatment, however, shows that quantum tunneling is much richer, necessitating deviations from the exponential decay in both the short- and long-time regimes [49,50]. Indeed, deviations from exponential decay were observed in the short-time regime in a pioneering experiment with cold atoms loaded into an accelerated optical lattice [51]. The deviations from purely exponential tunneling probabilities observed in this work are fundamentally different; they have their origin in the nonlinearity of the interactions. Nonlinearities also play a fundamental role in the tunneling of a BEC out of an external trap into the continuum [52,53]. In that case, however, the nonlinear Landau-Zener model cannot be applied. Our work is also fundamentally different from the nonexponential decay analyzed theoretically in Floquet-Bloch bands [54], where the emphasis lies on short-time deviations and oscillations due to a finite energy window and not due to nonlinear mean-field interactions.

Support by the National Science Foundation through Grants No. PHY-1806259 (Q. G. and D. B.) and No. PHY-1607495/PHY-1912540 (M. K. H. O., T. M. B., S. M., and P. E.) are gratefully acknowledged. This work used the OU Supercomputing Center for Education and Research (OSCER) at the University of Oklahoma (OU).

[1] L. Landau, Zur Theorie der Energieübertragung. II., Phys. Z. Sowjetunion **2**, 46 (1932).
[2] C. Zener, Non-adiabatic crossing of energy levels, Proc. R. Soc. A **137**, 696 (1932).
[3] B. Wu and Q. Niu, Nonlinear Landau-Zener tunneling, Phys. Rev. A **61**, 023402 (2000).
[4] O. Zobay and B. M. Garraway, Time-dependent tunneling of Bose-Einstein condensates, Phys. Rev. A **61**, 033603 (2000).
[5] J. Liu, L. Fu, B.-Y. Ou, S.-G. Chen, D.-I. Choi, B. Wu, and Q. Niu, Theory of non-linear Landau-Zener tunneling, Phys. Rev. A **66**, 023404 (2002).
[6] B. Wu, R. B. Diener, and Q. Niu, Bloch waves and bloch bands of Bose-Einstein condensates in optical lattices, Phys. Rev. A **65**, 025601 (2002).
[7] D. Diakonov, L. M. Jensen, C. J. Pethick, and H. Smith, Loop structure of the lowest Bloch band for a Bose-Einstein condensate, Phys. Rev. A **66**, 013604 (2002).
[8] E. J. Mueller, Superfluidity and mean-field energy loops: Hysteretic behavior in Bose-Einstein condensates, Phys. Rev. A **66**, 063603 (2002).
[9] M. Machholm, C. J. Pethick, and H. Smith, Band structure, elementary excitations, and stability of a Bose-Einstein condensate in a periodic potential, Phys. Rev. A **67**, 053613 (2003).
[10] O. Morsch, J. H. Müller, M. Cristiani, D. Ciampini, and E. Arimondo, Bloch Oscillations and Mean-Field Effects of Bose-Einstein Condensates in 1D Optical Lattices, Phys. Rev. Lett. **87**, 140402 (2001).
[11] M. Cristiani, O. Morsch, J. H. Müller, D. Ciampini, and E. Arimondo, Experimental properties of Bose-Einstein condensates in one-dimensional optical lattices: Bloch oscillations, Landau-Zener tunneling, and mean-field effects, Phys. Rev. A **65**, 063612 (2002).
[12] M. Jona-Lasinio, O. Morsch, M. Cristiani, N. Malossi, J. H. Müller, E. Courtade, M. Anderlini, and E. Arimondo, Asymmetric Landau-Zener Tunneling in a Periodic Potential, Phys. Rev. Lett. **91**, 230406 (2003).
[13] D. Witthaut, E. M. Graefe, and H. J. Korsch, Towards a generalized Landau-Zener formula for an interacting Bose-Einstein condensate in a two-level system, Phys. Rev. A **73**, 063609 (2006).
[14] A. Zenesini, C. Sias, H. Lignier, Y. Singh, D. Ciampini, O. Morsch, R. Mannella, E. Arimondo, A. Tomadin, and S. Wimberger, Resonant tunneling of Bose-Einstein condensates in optical lattices, New J. Phys. **10**, 053038 (2008).
[15] A. Zenesini, H. Lignier, G. Tayebirad, J. Radogostowicz, D. Ciampini, R. Mannella, S. Wimberger, O. Morsch, and E. Arimondo, Time-Resolved Measurement of Landau-Zener Tunneling in Periodic Potentials, Phys. Rev. Lett. **103**, 090403 (2009).
[16] Y.-A. Chen, S. D. Huber, S. Trotzky, I. Bloch, and E. Altman, Many-body Landau-Zener dynamics in coupled one-dimensional Bose liquids, Nat. Phys. **7**, 61 (2011).
[17] F. A. An, E. J. Meier, J. Ang'ong'a, and B. Gadway, Correlated Dynamics in a Synthetic Lattice of Momentum States, Phys. Rev. Lett. **120**, 040407 (2018).
[18] Y. Zhang, Z. Gui, and Y. Chen, Nonlinear dynamics of a spin-orbit-coupled Bose-Einstein condensate, Phys. Rev. A **99**, 023616 (2019).
[19] S. Eckel, J. G. Lee, F. Jendrzejewski, N. Murray, C. W. Clark, C. J. Lobb, W. D. Phillips, M. Edwards, and G. K. Campbell, Hysteresis in a quantized superfluid 'atomtronic' circuit, Nature (London) **506**, 200 (2014).
[20] J. Liu, B. Wu, and Q. Niu, Nonlinear Evolution of Quantum States in the Adiabatic Regime, Phys. Rev. Lett. **90**, 170404 (2003).
[21] J. C. Eilbeck, P. S. Lomdahl, and A. C. Scott, The discrete self-trapping equation, Physica (Amsterdam) **16D**, 318 (1985).
[22] V. M. Kenkre and D. K. Campbell, Self-trapping on a dimer: Time-dependent solutions of a discrete nonlinear Schrödinger equation, Phys. Rev. B **34**, 4959(R) (1986).
[23] A. H. Silver and J. E. Zimmerman, Quantum states and transitions in weakly connected superconducting rings, Phys. Rev. **157**, 317 (1967).
[24] K. Mullen, E. Ben-Jacob, and Z. Schuss, Combined Effect of Zener and Quasiparticle Transitions on the Dynamics of Mesoscopic Josephson Junctions, Phys. Rev. Lett. **60**, 1097 (1988).
[25] C. Ryu, P. W. Blackburn, A. A. Blinova, and M. G. Boshier, Experimental Realization of Josephson Junctions for an Atom SQUID, Phys. Rev. Lett. **111**, 205301 (2013).

[26] A. L. Fetter, Low-lying superfluid states in a rotating annulus, Phys. Rev. **153**, 285 (1967).
[27] E. Hoskinson, Y. Sato, I. Hahn, and R. E. Packard, Transition from phase slips to the Josephson effect in a superfluid ^{4}He weak link, Nat. Phys. **2**, 23 (2006).
[28] A. Ramanathan, K. C. Wright, S. R. Muniz, M. Zelan, W. T. Hill III, C. J. Lobb, K. Helmerson, W. D. Phillips, and G. K. Campbell, Superflow in a Toroidal Bose-Einstein Condensate: An Atom Circuit with a Tunable Weak Link, Phys. Rev. Lett. **106**, 130401 (2011).
[29] K. C. Wright, R. B. Blakestad, C. J. Lobb, W. D. Phillips, and G. K. Campbell, Driving Phase Slips in a Superfluid Atom Circuit with a Rotating Weak Link, Phys. Rev. Lett. **110**, 025302 (2013).
[30] D.-I. Choi and Q. Niu, Bose-Einstein Condensates in an Optical Lattice, Phys. Rev. Lett. **82**, 2022 (1999).
[31] D.-I. Choi and B. Wu, To detect the looped Bloch bands of Bose-Einstein condensates in optical lattices, Phys. Lett. A **318**, 558 (2003).
[32] S. B. Koller, E. A. Goldschmidt, R. C. Brown, R. Wyllie, R. M. Wilson, and J. V. Porto, Nonlinear looped band structure of Bose-Einstein condensates in an optical lattice, Phys. Rev. A **94**, 063634 (2016).
[33] G. Watanabe, B. P. Venkatesh, and R. Dasgupta, Nonlinear phenomena of ultracold atomic gases in optical lattices: Emergence of novel features in extended states, Entropy **18**, 118 (2016).
[34] See Supplemental Material at http://link.aps.org/supplemental/10.1103/PhysRevLett.125.213401 for selected properties of the Hamiltonian $\hat{H}_{\mathrm{TS}}$; the Supplemental Material also details the derivation of the two-state model, provides additional information pertinent to Fig. 2, gives the formula for the tunneling probabilities used to plot the gray-shaded region in Fig. 3, shows extended datasets for the mean-field-dominated regime, discusses the tunneling probabilities in the lattice-coupling-strength-dominated regime, and shows integrated densities at the end of the ramp, which includes Refs. [5,35,36].
[35] Y. Castin and R. Dum, Bose-Einstein Condensates in Time Dependent Traps, Phys. Rev. Lett. **77**, 5315 (1996).
[36] Q. Guan, T. M. Bersano, S. Mossman, P. Engels, and D. Blume, Rabi oscillations and Ramsey-type pulses in ultracold bosons: Role of interactions, Phys. Rev. A **101**, 063620 (2020).
[37] O. Morsch and M. Oberthaler, Dynamics of Bose-Einstein condensates in optical lattices, Rev. Mod. Phys. **78**, 179 (2006).
[38] E. Peik, M. B. Dahan, I. Bouchoule, Y. Castin, and C. Salomon, Bloch oscillations of atoms, adiabatic rapid passage, and monokinetic atomic beams, Phys. Rev. A **55**, 2989 (1997).
[39] C. Hamner, Y. Zhang, M. A. Khamehchi, M. J. Davis, and P. Engels, Spin-Orbit-Coupled Bose-Einstein Condensates in a One-Dimensional Optical Lattice, Phys. Rev. Lett. **114**, 070401 (2015).
[40] The value of the scattering length is taken from M. A. Khamehchi, Y. Zhang, C. Hamner, T. Busch, and P. Engels, Measurement of collective excitations in a spin-orbit-coupled Bose-Einstein condensate, Phys. Rev. A **90**, 063624 (2014).
[41] G. Sun, X. Wen, M. Gong, D.-W. Zhang, Y. Yu, S.-L. Zhu, J. Chen, P. Wu, and S. Han, Observation of coherent oscillation in single-passage Landau-Zener transitions, Sci. Rep. **5**, 8463 (2015).
[42] M. Albiez, R. Gati, J. Fölling, S. Hunsmann, M. Cristiani, and M. K. Oberthaler, Direct Observation of Tunneling and Nonlinear Self-Trapping in a Single Bosonic Josephson Junction, Phys. Rev. Lett. **95**, 010402 (2005).
[43] S. Levy, E. Lahoud, I. Shomroni, and J. Steinhauer, The a.c. and d.c. Josephson effects in a Bose-Einstein condensate, Nature (London) **449**, 579 (2007).
[44] L. Fallani, L. De Sarlo, J. E. Lye, M. Modugno, R. Saers, C. Fort, and M. Inguscio, Observation of Dynamical Instability for a Bose-Einstein Condensate in a Moving 1D Optical Lattice, Phys. Rev. Lett. **93**, 140406 (2004).
[45] M. Cristiani, O. Morsch, N. Malossi, M. Jona-Lasinio, M. Anderlini, E. Courtade, and E. Arimondo, Instabilities of a Bose-Einstein condensate in a periodic potential: An experimental investigation, Opt. Express **12**, 4 (2004).
[46] B. Wu and Q. Niu, Landau and dynamical instabilities of the superflow of Bose-Einstein condensates in optical lattices, Phys. Rev. A **64**, 061603(R) (2001).
[47] A. Smerzi, A. Trombettoni, P. G. Kevrekidis, and A. R. Bishop, Dynamical Superfluid-Insulator Transition in a Chain of Weakly Coupled Bose-Einstein Condensates, Phys. Rev. Lett. **89**, 170402 (2002).
[48] B. Wu and Q. Niu, Superfluidity of Bose-Einstein condensate in an optical lattice: Landau-Zener tunneling and dynamical instability, New J. Phys. **5**, 104 (2003).
[49] L. Fonda, G. C. Ghirardi, and A. Rimini, Decay theory of unstable quantum systems, Rep. Prog. Phys. **41**, 587 (1978).
[50] P. T. Greenland, Seeking non-exponential decay, Nature (London) **335**, 298 (1988).
[51] S. R. Wilkinson, C. F. Bharucha, M. C. Fischer, K. W. Madison, P. R. Morrow, Q. Niu, B. Sundaram, and M. G. Raizen, Experimental evidence for non-exponential decay in quantum tunneling, Nature (London) **387**, 575 (1997).
[52] S. Potnis, R. Ramos, K. Maeda, L. D. Carr, and A. M. Steinberg, Interaction-Assisted Quantum Tunneling of a Bose-Einstein Condensate Out of a Single Trapping Well, Phys. Rev. Lett. **118**, 060402 (2017).
[53] X. Zhao, D. A. Alcala, M. A. McLain, K. Maeda, S. Potnis, R. Ramos, A. M. Steinberg, and L. D. Carr, Macroscopic quantum tunneling escape of Bose-Einstein condensates, Phys. Rev. A **96**, 063601 (2017).
[54] A. Cao, C. J. Fujiwara, R. Sajjad, E. Q. Simmons, E. Lindroth, and D. Weld, Probing nonexponential decay in Floquet-Bloch bands, Z. Naturforsch. **75**, 443 (2020).